International Journal of Adhesion & Adhesives 32 (2012) 15–22

Contents lists available at SciVerse ScienceDirect

International Journal of Adhesion & Adhesives

journal homepage: www.elsevier.com/locate/ijadhadh

Effects of low-temperature curing on physical behavior of cold-curing epoxy adhesives in bridge construction

Omar Moussa, Anastasios P. Vassilopoulos *, Thomas Keller

Composite Construction Laboratory (CCLab), Ecole Polytechnique Fédérale de Lausanne, (EPFL), Station 16, Bâtiment BP, CH-1015 Lausanne, Switzerland

ARTICLE INFO

Article history:
Accepted 4 September 2011
Available online 12 September 2011

Keywords:
Epoxy/epoxides
Thermal analysis
Cure/hardening
Glass transition

ABSTRACT

The effect of low-temperature curing on the physical characteristics of a commercial cold-curing epoxy adhesive was experimentally and analytically investigated with a view to a potential application in bridge construction in winter. Curing at low temperatures of 5–10 °C took place but the curing process was significantly decelerated due to material vitrification and the associated diffusion-controlled reaction. Existing dynamic and isothermal curing models developed for hot-curing adhesives proved to be applicable to simulate the curing behavior. However, a heating rate-dependent pre-exponential factor and diffusion control had to be taken into account. The relationship between the glass transition temperature and the curing degree could also be described by models developed for hot-curing adhesives. However, at low temperatures, the relationship was curing temperature-dependent, something which had to be taken into account in the modeling in order to provide accurate simulation.

1. Introduction

Structural adhesive bonding is well-established in the aircraft and automotive industries and mechanical engineering, where, in most cases, joints can be fabricated indoors under controlled conditions. In the civil engineering domain, however, load-bearing structures are normally erected on-site in outdoor conditions, i.e. joint fabrication is exposed to varying outdoor temperatures and humidity [1–2]. Consequently, and due to the normal large scale of the structural components, cold-curing adhesives can be used, unlike in other fields where hot-curing adhesives are applied indoors. Particularly in winter, long periods of very low temperatures are frequent [3], during which on-site joining of structural components must remain possible however.

Due to these harsh environmental conditions, structural adhesive bonding is not yet widely used in civil engineering structures, although it also offers many potential advantages in this field, the most important being the ease of joining different materials (e.g. steel to concrete) and components of complex forms and the rapidity of connection, which is beneficial in bridge construction to prevent extensive traffic interruptions [2]. Bridge construction is also the field in which structural or semi-structural adhesive joining has mainly been applied in the past. Connections between segments of concrete bridges, between concrete bridge decks and steel girders or joints of steel trusses (with additional prestressed bolts) have been adhesively bonded using cold-curing epoxy adhesives [2,4–6]. More recent and frequent applications involve the strengthening of existing concrete, steel or timber structures by means of adhesively-bonded carbon fiber-reinforced (CFRP) laminates [7,8].

For the wider application of adhesive joints in bridges, an understanding of the curing behavior and associated development of the mechanical properties of cold-curing adhesives, particularly when exposed to low temperatures, must be acquired. The curing rate produced at low-curing temperatures must be predicted in order to decide when a bridge can be opened for traffic for example. Although adhesive curing theories do exist, they were developed for hot-curing adhesives only and the proof of their applicability to describe the physical behavior of cold-curing adhesives, especially at low temperatures, is still lacking.

The main material characteristics involved and of interest are the curing degree, α, (representing the cross-linking of the adhesive molecules) and the glass transition temperature, T_g, beyond which mechanical properties decrease. The relationship between the curing temperature, T_{cure}, and T_g (which increases during curing) not only defines the physical state of the material (liquid, rubbery or glassy) but also the reaction rate during the curing process [9,10]:

$T_{cure} > T_g$: the reaction proceeds rapidly at a rate driven by chemical kinetics.
$T_{cure} \approx T_g$: vitrification takes place, i.e. material solidifies.
$T_{cure} < T_g$: the reaction rate decelerates and becomes diffusion-controlled.

* Corresponding author. Tel.: +41 21 6936393; fax: +41 21 6936240.
E-mail address: anastasios.vasilopoulos@epfl.ch (A.P. Vassilopoulos).

0143-7496/$ - see front matter © 2011 Elsevier Ltd. All rights reserved.
doi:10.1016/j.ijadhadh.2011.09.001

Based on the above analysis, the effect of low-temperature curing on the physical states of a commercial cold-curing epoxy adhesive (Sikadur-30) was experimentally investigated. Temperatures down to 5 °C were taken into account. The applicability of existing curing models–previously developed for hot-curing adhesives–to the present cold-curing adhesive was examined. The results of this work and their impact on the design and fabrication of bridge joints are discussed in this paper.

2. Experimental investigation

2.1. Adhesive description

The adhesive used was the Sikadur-30 adhesive from Sika Schweiz AG, a two-component thixotropic, solvent-free epoxy-based resin used to join steel and concrete components. The adhesive is mixed at ambient temperature at a ratio of 3:1 by weight of the respective constituents (resin and hardener). The resin contains silica quartz fillers. Their size between 200 and 500 μm and weight fraction of approximately 55% were determined using optical microscopy, as shown in Fig. 1, and resin burn-off. According to the manufacturer's data sheets, the tensile strength and modulus of elasticity for fully cured materials are 31 MPa and 11.2 GPa, respectively (according to DIN 53 455 and ISO 527, respectively). The glass transition temperature of specimens cured at 45 °C during 7 days is 62 °C (resulting from a torsion pendulum test).

2.2. Experimental setup

A heat-flux differential scanning calorimeter (DSC-TA Q100) connected to a thermal analyzer was used to detect the heat released during the cure reaction. The equipment is supplied by a liquid nitrogen cooling system providing an inert atmosphere, thus allowing the DSC cell to reach very low temperature ranges.

The weight of each sample was measured prior to scanning by a microbalance. Sample weight ranged between 5 and 10 mg according to preliminary tests carried out to specify the heating rate, curing temperature and suitable sample weight ranges. The samples were placed in a steel pan covered with a lid and sealed with a manual press. An empty steel pan of the same type and size was used as a reference during every scan. Data acquisition was performed using the accompanying software (TA Analysis).

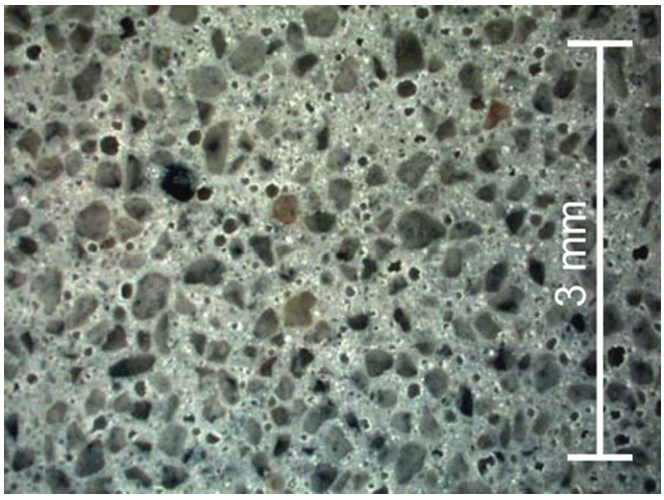

Fig. 1. Optical microscopy showing adhesive filler size.

2.3. Experimental program

Uncured samples were used to determine (a) the total heat of reaction released during a complete curing process of a dynamic scan and (b) the maximum heat of reaction reached at different isothermal temperatures.

Dynamic scans were conducted in the temperature range of −50 °C to 250 °C at constant heating rates of 2.5, 5, 10, 15 and 20 °C/min. By extending the scanning temperature range, the decomposition reaction of the material was found to initiate at a temperature of 297 ± 2 °C (result from 3 scans at 15 °C/min).

Isothermal scans were conducted at temperatures ranging between 5 and 80 °C. This range was chosen in accordance with the planned bridge application. Samples were then placed in the DSC cell and equilibrium at the target isothermal temperature was reached in the sample holder with a rate of 20 °C/min. The samples were then scanned isothermally until the heat flow curve approached a plateau.

When samples were scanned at high temperatures above T_g, part of the initial data was not recorded. The curing process was too rapid and part of the reaction heat was released before detection by the calorimeter. Furthermore, at low curing temperatures of 5, 10 and 25 °C, a large scatter in the results was obtained. Therefore, an alternative method, which proved to be efficient in [11], was used to determine the development of the curing degree at low (5, 10 and 25 °C) and high (70 °C) curing temperatures. The samples were pre-conditioned in a climate chamber (according to ASTM D618-05) at different curing temperatures (5, 10, 25, and 70 °C) during different time periods, t_{cure}, (ranging from several minutes at the highest temperature to 10 days at the lowest temperature). Constant humidity (50 ± 2%) was maintained in order to eliminate any possible effect on the curing process. After removal from the chamber, the samples were rapidly quenched in liquid nitrogen to stop the reaction. The residual cure and the corresponding glass transition temperature of the partially cured samples were then obtained by running a dynamic scan. Three samples were investigated for each combination (T_{cure} and t_{cure}).

This procedure was also used to investigate the development of the glass transition temperature as a function of time as well as the relationship between the glass transition temperature and the curing degree. T_g was determined as the midpoint of the step in the curve preceding the exhibited curing exotherm during the dynamic scan, according to ASTM E 2602. In some cases, at a low curing degree and low T_g (at short t_{cure}), difficulty in detecting the

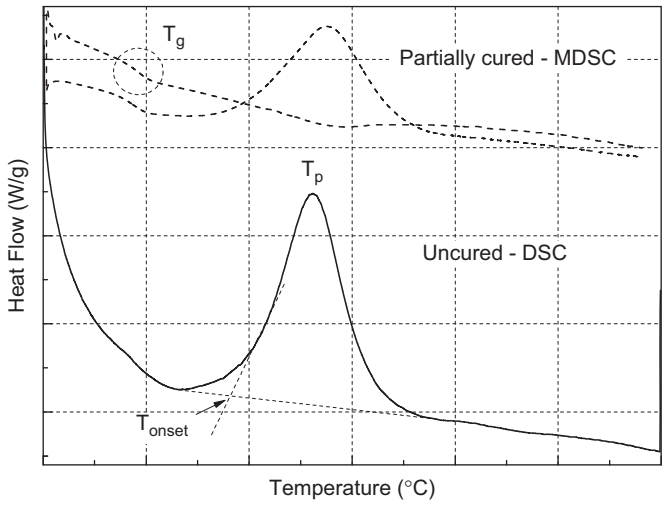

Fig. 2. Heat flow vs. temperature in typical DSC and MDSC scans of uncured and partially cured samples.

corresponding T_g was encountered. Modulated DSC (MDSC) was then used to separate reversible and non-reversible reactions, which enabled the T_g to be detected from the reversible heat capacity (see Fig. 2). Modulation was carried out at an amplitude of ± 0.5 °C every 60 s and nitrogen was used as the purge gas.

A half-life validation (according to ASTM E-698) was performed to assess the results. A sample was preconditioned at the determined half-life temperature, T_{h-l}, for 60 min in the DSC chamber and then rapidly quenched in liquid nitrogen to stop the reaction. The sample was subsequently scanned at 10 °C/min (an intermediate heating rate) between -50 and 250 °C.

3. Kinetic analysis of experimental results

Typical DSC and MDSC scans of uncured and partially cured samples are presented in Fig. 2 showing the thermal transitions (glass transition and curing) and curve parameters (peak and onset of cure temperatures). The change in heat flow vs. temperature and time during cure at different heating rates is shown in Fig. 3a and b. The peak temperature, T_p, the onset of cure temperature, T_{onset} (defined according to ASTM E2041), and the shape of the exotherm were heating rate-dependent. The value of the heat released was determined by integrating heat flow vs. time under the exotherm along a straight base line, as shown in Fig. 3b. This heat of reaction, ΔH_T, was independent of the heating rate, see Table 1 (95.1 ± 1.56 J/g). The scatter of samples scanned at the same heating rate was examined by scanning three samples at 15 °C/min and was found to be small (95.5 ± 0.5 J/g).

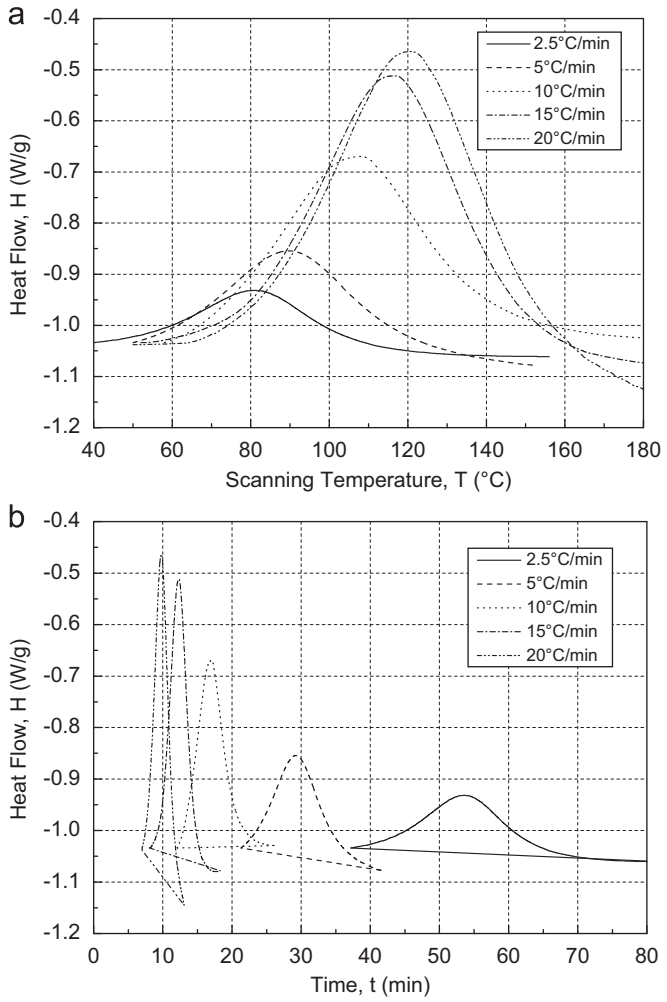

Fig. 3. Heat flow at different heating rates during dynamic scanning as function of (a) temperature and (b) time (between onset and end of cure).

The heat flow vs. time of isothermal scans at temperatures between 35 and 60 °C is shown in Fig. 4. Reducing the curing temperature delayed the maximum heat flow due to the deceleration of the reaction and corresponding movement of the particles. Similar behavior was exhibited at temperatures below 35 °C, however the curves are not presented in Fig. 4 due to the large exhibited scatter, as mentioned in Section 2.3. The heat released during isothermal scanning, ΔH_{iso}, was calculated as the area under each isothermal curve considering the plateau as a horizontal base line; the results are listed in Table 2.

Based on dynamic and isothermal results, the curing degree, α, was calculated as $\Delta H_{iso}/\Delta H_T$. The resulting values vs. time are shown in Fig. 5 for the two experimental methods (pre-conditioning and subsequent dynamic scans vs. isothermal scans, see Section 2.3). At high temperatures, full curing was attained after a few hours. At lower temperatures curing was delayed: at 5 °C for example, 70% of

Table 1
Dynamic scanning results at different heating rates.

Parameter	dT/dt (°C/min)				
	2.5	5	10	15	20
ΔH_T (J/g)	92.64	94.50	96.36	95.52	96.36
T_{onset} (°C)	41.4	50.5	58.0	73.6.0	77.0
T_p (°C)	80.8	89.7	107.8	116.8	120.8
α_p (%)	0.49	0.46	0.54	0.54	0.49
$(d\alpha/dt)_p$ (min^{-1})	0.069	0.12	0.22	0.33	0.39
$(d\alpha/dT)_p$ ($°C^{-1}$)	0.0278	0.024	0.022	0.022	0.019

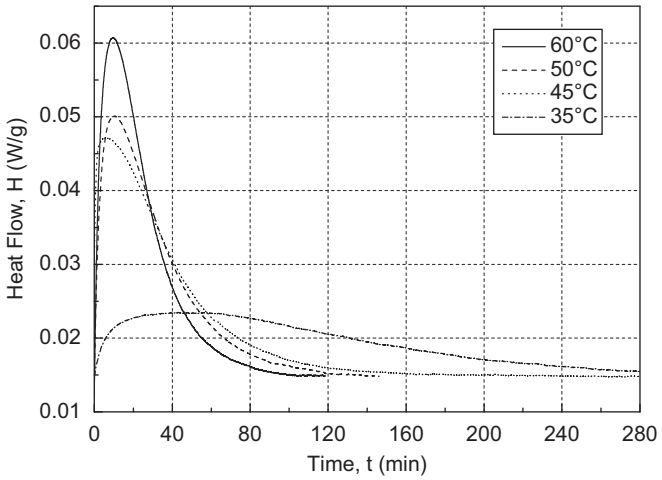

Fig. 4. Heat flow at different isothermal curing temperatures.

Table 2
Isothermal scanning results at different temperatures until onset of diffusion control.

Parameter	T_{cure} (°C)							
	5[a]	10[a]	25[a]	35	45	50	60	70[a]
ΔH_{iso} (J/g)	–	–	–	91.54	94.44	96.36	96.36	–
α (%)	–	–	–	0.95	0.98	1	1	–
t (h)	–	–	–	3.73	2.42	2.05	1.58	–
t_{50} (h)	11.85	6.67	1.54	0.97	0.45	0.4	0.38	0.15

[a] Results from alternative pre-conditioning method.

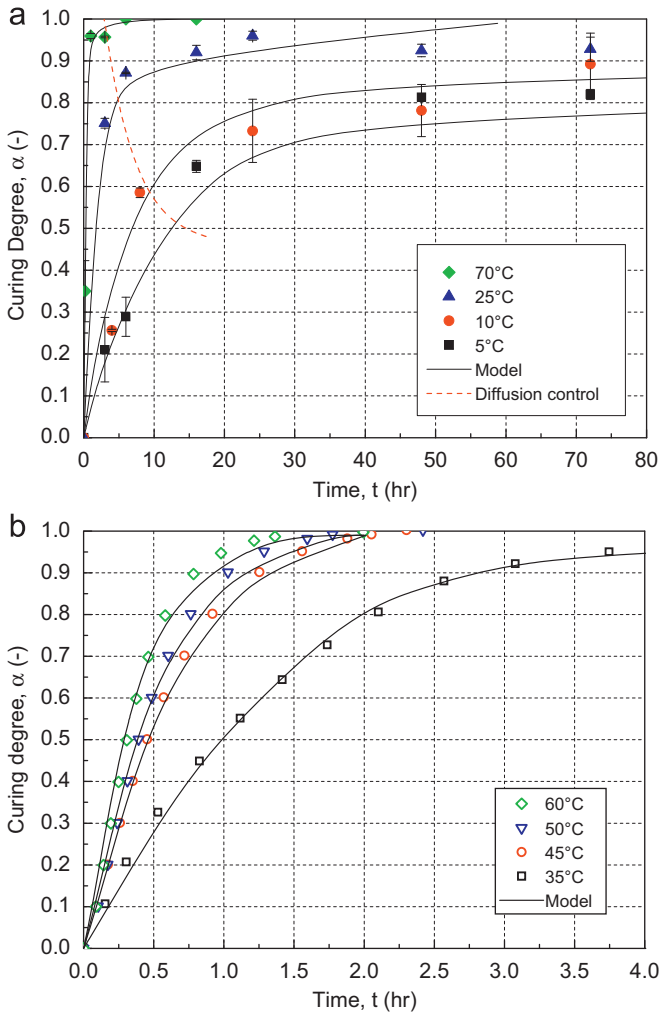

Fig. 5. Curing degree vs. time, (a) using pre-conditioning method and (b) from DSC isothermal scans.

curing required almost one day and 90% was attained after 3 days at 10 °C. Fig. 5a also shows the onset of diffusion control (for derivation see below) after which curing was further delayed.

According to the time required to attain 50% curing, t_{50} (see Table 2), the 60-min half-life temperature was found to be 34 °C. The integrated peak area of the partially cured sample represented 49.7% of the peak area of the uncured sample and was thus within the standard range (50 ± 0.5%). The validity of the DSC results was therefore confirmed.

4. Kinetic modeling and discussion

Until now, research has been focused on the cure kinetics of hot-curing epoxies [12–18]. Determination of the kinetic parameters has been conducted either by means of a series of isothermal experiments [12–16] or dynamic scans [16–18]. These works focused on temperature ranges above 50 °C [13,14,16]. Dynamic and isothermal modeling developed for hot-curing adhesives are applied in the following to describe the experimental responses of the cold-curing adhesive.

4.1. Dynamic modeling

The basic modeling equation relates the curing rate, $d\alpha/dt$, at a specific temperature, to a function of the curing (or chemical conversion) degree, α, which depends on the concentration of the reactants, $f(\alpha)$:

$$\frac{d\alpha}{dt} = kf(\alpha) \tag{1}$$

where k is the rate constant. Basically, resins may exhibit two different behaviors, nth order or autocatalytic [15]. The main difference is that nth order resins exhibit a cure rate peak at the beginning of the reaction, while autocatalytic resins show a delayed peak, which occurs during the curing process.

Based on the responses shown in Fig. 4, which exhibited a delayed peak, an autocatalytic behavior was assumed, as follows

$$f(\alpha) = \alpha^m(1-\alpha)^n \tag{2}$$

where n and m are the reaction orders (with $m+n$ being the overall reaction order). Furthermore, the rate constant is temperature-dependent, following the Arrhenius law:

$$k = Ae^{-E_a/RT} \tag{3}$$

where $A$is the pre-exponential factor, $E_a$is the activation energy (J/mol), R=8.314 J/mol K is the universal gas constant and T is the temperature (K). Substituting k in Eq. (1) by Eq. (3) results in the rate equation:

$$\frac{d\alpha}{dt} = Ae^{-E_a/RT}f(\alpha) \tag{4}$$

The kinetic parameters n, m, A and E_a were determined by fitting the experimental results to the autocatalytic model, as demonstrated in [17] for commercial epoxy prepregs. A method based on the Kissinger and Ozawa methods [19–20] was used. Eq. (4) was rearranged by multiplying the left hand side by dT/dT and taking the natural logarithm of both sides as follows

$$\ln\left(\frac{dT}{dt}\right) = \ln(A) - \ln\left(\frac{d\alpha}{dT}\right) + \ln(f(\alpha)) - \frac{E_a}{RT} \tag{5}$$

where dT/dt is the heating rate. At peak temperature, T_p, the derivative of the curing rate with respect to temperature equals zero, which means that the derivative of the curing degree with respect to temperature is a constant value regardless of the heating rate. Furthermore, since at peak temperature the change in $\ln f(\alpha)$ with respect to the heating rate is negligible compared to that in $\ln A$ [17], the general linear form of the previous equation can be written as

$$\ln\left(\frac{dT}{dt}\right) = K + \left(\frac{-E_a}{R}\right)\frac{1}{T_p} \tag{6}$$

where K is the intercept of Eq. (6). An average activation energy of E_a=56.3 kJ/mol was calculated from the slope of the plot $\ln(dT/dt)$ vs. $1000/T_p$, see Table 3. Furthermore, the change in activation energy during the whole curing process was obtained from isoconversional plots $\ln(dT/dt)$ vs. $1000/T$ at different curing degrees, as shown in Fig. 6. It decreased from 65 kJ/mol at the beginning of the curing process to 57 kJ/mol and then slightly increased due to the energy required to increase the mobility of both the reactants and products during the late stages of the curing process. Similar behavior was found for other materials [17,18], particularly in the later stages of curing.

An average pre-exponential factor A was obtained from the intercept of Eq. (6), see Table 3. Based on this value and Sun et al. [17], heating rate-specific values, A_f, were obtained as follows

$$A_f = C_f \cdot A_{av} = C_f \frac{e^K(d\alpha/dt)_p}{\alpha_p^m(1-\alpha_p)^n} \tag{7}$$

where C_f is the heating rate-dependent correction factor of A_{av}, and $(d\alpha/dt)_p$ and α_p are the curing rate and curing degree at peak, respectively, as given in Table 1. Integerating Eqs. (7) and (2) in the basic curing rate Eq. (4), the curing rate for an autocatalytic

Table 3
Kinetic parameters obtained from autocatalytic dynamic model.

Model	Parameter	*dT/dt* (°C/min)					
		2.5	5	10	15	20	R^2
Kissinger and Ozawa	E_a (kJ/mol)	←		56.3	→		0.99
	A (min^{-1})	←		44431700	→		0.97
Modified Kissinger and Ozawa	m	0.52	0.28	0.04	0.27	0.12	
	n	1.99	1.81	1.16	1.47	1.49	
	C_f	0.899	1.124	0.897	0.909	0.982	0.97
	A_f (min^{-1})	77732893	58040782	27754751	40959771	31786834	

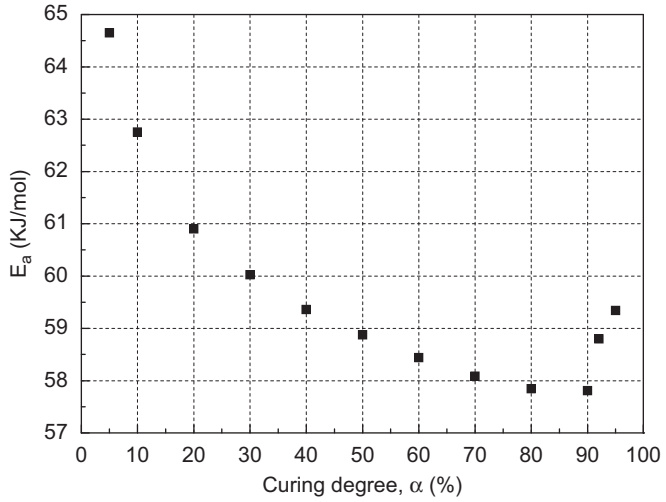

Fig. 6. Activation energy from isoconversional plots vs. curing degree.

model yields to:

$$\frac{d\alpha}{dt} = C_f \cdot e^K \left(\frac{d\alpha}{dT}\right)_p e^{-(E_a/RT)} \frac{\alpha^m(1-\alpha)^n}{\alpha_p^m(1-\alpha_p)^n} \tag{8}$$

The correction factors C_f as well as the reaction orders, m and n, were determined from Eq. (8) using the multiple non-linear least square regression method based on the Levenberg–Marquardt algorithm; the results are shown in Table 3.

Once the kinetic parameters A, E_a, m and n had been estimated, the curing degree was calculated as a function of the temperature by solving Eq. (9) numerically using the fourth-order Runge–Kutta method.

$$\frac{d\alpha}{dT} = \frac{A_f}{dT/dt} e^{-(E_a/RT)} \alpha^m(1-\alpha)^n \tag{9}$$

The results for the heating rates of 2.5 and 20 °C/min with and without modification of the pre-exponential factor are shown in Fig. 7a. The modeling curves compare well to the experimental results, particularly with modification of the pre-exponential factor. The late stages of curing at 2.5 °C/min were only slightly underestimated, most probably due to disregarding the term $\ln f(\alpha)$ in Eq. (5). At 2.5 °C/min, the term $\ln f(\alpha)$ was found to be approximately 26% of the term $\ln A$ at 90% of cure, which is not really negligible. Similarly, Fig. 7b shows the curing rate vs. temperature for the same heating rates. Again, the autocatalytic model with modification of the pre-exponential factor provides good and more accurate results than the model without modification.

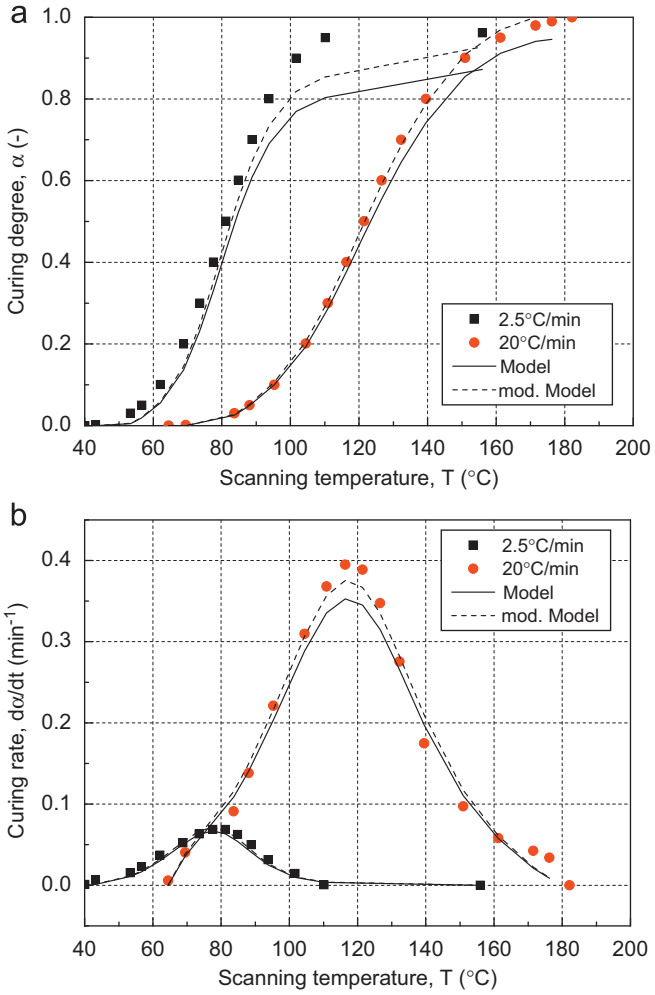

Fig. 7. (a) Curing degree and (b) curing rate vs. temperature: comparison of experimental and autocatalytic model results (with and without modified pre-exponential factor).

4.2. Isothermal modeling

A more general model than Eq. (1) was used for the isothermal modeling, which takes non-zero values of the initial curing rate into account

$$\frac{d\alpha}{dt} = (k_1 + k_2\alpha^m)(1-\alpha)^n \tag{10}$$

where k_1 and k_2 are curing rate constants with k_1 being the value at the beginning of the reaction at $t=0$.

Table 4
Kinetic parameters obtained from autocatalytic isothermal model.

T (°C)	K_1 (min^{-1})	K_2 (min^{-1})	n	m	$m+n$	R^2	E_{a1} (kJ/mol)	A_1 (min^{-1})	R^2	E_{a2} (kJ/mol)	A_2 (min^{-1})	R^2
60	0.0192	0.0578	1.291	0.553	1.843	0.97						
50	0.0160	0.0435	1.348	0.595	1.943	0.99						
45	0.0143	0.0378	1.408	0.650	2.058	0.99						
35	0.00948	0.0278	1.758	1.168	2.926	0.98	36.6	13226.8	0.97	19.2	54.6	0.97
25	0.0065	0.0251	2.010	1.738	3.748	0.99						
10	0.0025	0.0186	2.950	2.610	5.560	0.98						
5	0.00137	0.0124	3.130	2.720	5.850	0.97						

Table 5
Diffusion control parameters obtained from autocatalytic isothermal model.

T (°C)	α_c	C	R^2
45	0.98	191.78	0.98
35	0.91	137.91	0.93
25	0.84	72.30	0.95
10	0.58	25.25	0.94
5	0.52	11.93	0.95

In a first step, Eq. (10) was fitted to the experimental data of curing rate vs. curing degree at each of the isothermal temperatures to obtain the rate constants and reaction orders (k_1, k_2, n and m). Results at 70 °C (clearly above T_g), were not taken into account. A non-linear least-square regression analysis was used as proposed in [13]. The value of the overall reaction order ($m+n$) decreased with increasing temperature, see Table 4, which is in contrast to the work, which assume this value as being constant ($m+n=2$ in [21]). Subsequently, by plotting the logarithms of the rate constants, $\ln k_1$ *and* $\ln k_2$, vs. *1000/T*, the activation energies, E_{a1}, E_{a2}, and logarithms of the pre-exponential factors, $\ln A_1$ and $\ln A_2$, were obtained from the slopes and the intercepts, respectively, see Table 4.

Approaching the glassy state, the cure reaction became diffusion-controlled, i.e. the movement of the reactants was slowed down and also hindered by the already formed chains. To take this effect into account, an extension of Eq. (10) by a diffusion control factor was proposed by Chern and Phoehlein [14] and applied as follows

$$\frac{d\alpha}{dt} = (k_1 + k_2\alpha^m)(1-\alpha)^n \frac{1}{1+e^{C(\alpha-\alpha_c)}} \quad (11)$$

where C is an empirical constant and α_c is the critical curing degree at which diffusion control initiates. To obtain these two parameters (which are curing temperature-dependent), the experimental results were non-linearly re-fitted with the already known kinetic parameters (from fitting according to Eq. (10)). The resulting values, presented in Table 5, show that the critical curing degree decreases when the curing temperature is decreased. At high temperatures (>50 °C), diffusion control is no longer relevant ($\alpha_c \to 1.0$).

A comparison between the experimental and the predicted curing degree according to Eq. (11) vs. time shows good agreement, as demonstrated in Fig. 5a and b. The values at 5 °C curing temperature are only slightly underestimated. The onsets of diffusion control (the critical curing degrees according to Table 5) are also shown.

The relationship between the curing rate and the curing degree is presented in Fig. 8 for temperatures between 5–60 °C. Experimental results were accurately simulated by the selected autocatalytic model as shown in Fig. 8. At higher curing temperatures (>35 °C), the maximum curing rate occurred at a curing degree of approximately 20%, nevertheless, at lower curing temperatures (<35 °C) the curves exhibited a negative (decreasing) slope in the early curing stages when m became >1 (see Table 4 and [13]) followed by a second peak at around 20% curing degree.

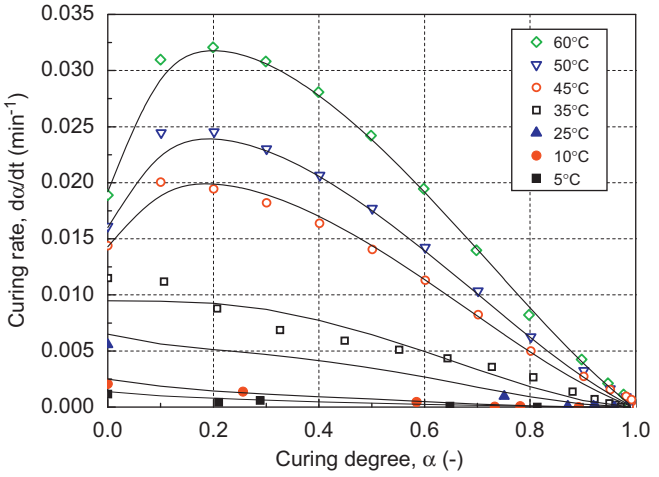

Fig. 8. Curing rate vs. curing degree: comparison of experimental and autocatalytic model results for different isothermal temperatures.

5. Glass transition temperature

The development of the glass transition temperature, T_g, during curing and the relationship to the curing degree was extensively investigated for hot-curing adhesives [10,22–25] and corresponding models were developed [10] whose applicability for cold-curing adhesives will be examined in the following.

The observed development of T_g vs. time, up to around 3 days, is shown in Fig. 9. At 70 °C curing temperature, a plateau was reached (at approx. 56 °C) after a few hours, which was however clearly below the 62 °C value given in the manufacturer's datasheet. T_g development at lower temperatures was much slower: at 5 °C, for example, around 50% of the maximum value was reached after only 3 days. The development decelerated when diffusion control and corresponding vitrification started, i.e. when T_g equaled T_{cure}. Similarly to Fig. 5a, the corresponding onset of diffusion control (or vitrification) is shown in Fig. 9 (expressed as $T_g = T_{cure}$ in this case).

A model to describe the T_g vs. α relationship (independent of the curing temperature in this case) was proposed by DiBenedetto

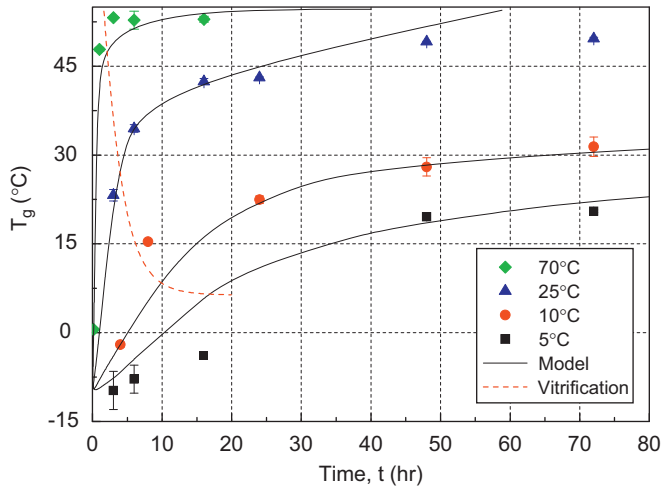

Fig. 9. Glass transition temperature vs. time for samples partially cured at different temperatures.

[26] as follows

$$\frac{T_g - T_{go}}{T_{go}} = \frac{(\varepsilon_\infty/\varepsilon_o - c_\infty/c_o)x}{1-(1-c_\infty/c_o)x} \tag{12}$$

where x being the crosslink density (defined as the fraction of all segments that are crosslinked), ε the lattice energy, c the segmental mobility and subscripts "0" and "∞" refer to the uncured and fully cured resin, respectively. A modified version of the DiBenedetto equation replaces x by the curing degree, α, as follows [22]

$$\frac{T_g - T_{go}}{T_{g\infty} - T_{go}} = \frac{\lambda\alpha}{1-(1-\lambda)\alpha} \tag{13}$$

with λ as an adjustable structure-dependent parameter, equal to $\Delta C_{p\infty}/\Delta C_{po}$, where $\Delta C_{p\infty}$ and ΔC_{po} are the differences in heat capacity between the glassy and rubbery/liquid states at full conversion and zero conversion, respectively [24].

A further model, based on thermodynamics and proposed by Couchman and Karasz [27], was adopted by Venditti and Gillham [24] and assumes that the system, at a curing degree α, is a mixture of unreacted end segments with concentration $(1-\alpha)$ and $T_g = T_{go}$, and reacted end segments with concentration α and $T_g = T_{g\infty}$:

$$\ln(T_g) = \frac{(1-\alpha)\ln(T_{go}) + \lambda\alpha\ln(T_{g\infty})}{(1-\alpha)+\lambda\alpha}. \tag{14}$$

Fitting Eqs. (13) and (14) to the experimental data resulted in the λ-values listed in Table 6, which also shows the experimental value calculated as defined previously. There is good agreement between the three values, which also lie within the range obtained for hot-curing epoxy systems (0.16–0.69) [24]. The corresponding curves are shown in Fig. 10 and show good agreement with the experimental results. However, the experimental data exhibited a significant dependency on the curing temperature (lowest T_g values at 5 °C), which could not be captured by the models. This is due to the early vitrification of the material followed by deceleration of the reaction, which becomes controlled by diffusion. In addition, the activation energy is not sufficient to cause secondary amines and sterical hindered amines to react.

To take the curing time dependency into account, Eq. (13) was fitted to the results of each curing temperature separately. The resulting changes in λ with curing temperature are shown in Fig. 11. Taking this result into consideration, the development of T_g over time, shown in Fig. 9, was modeled and good agreement to the experimental results was obtained.

Table 6
Fitted and experimental λ values.

Method	λ	R^2
Pascault and Williams	0.32	0.96
Venditti Gillham	0.36	0.95
DSC	0.33 ± 0.15	

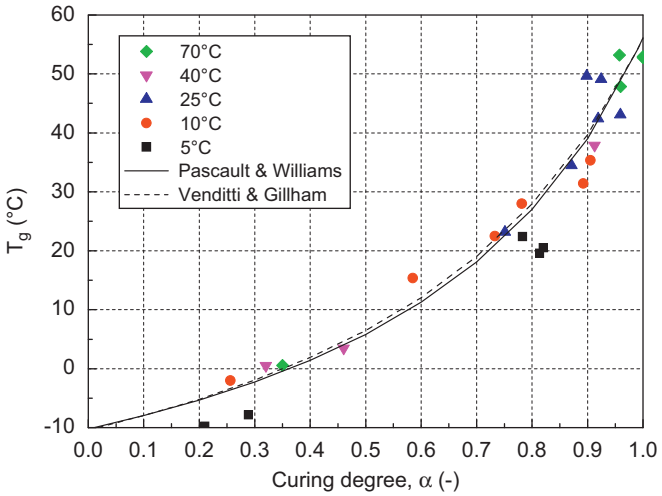

Fig. 10. Glass transition temperature vs. curing degree for partially cured specimens at different temperatures.

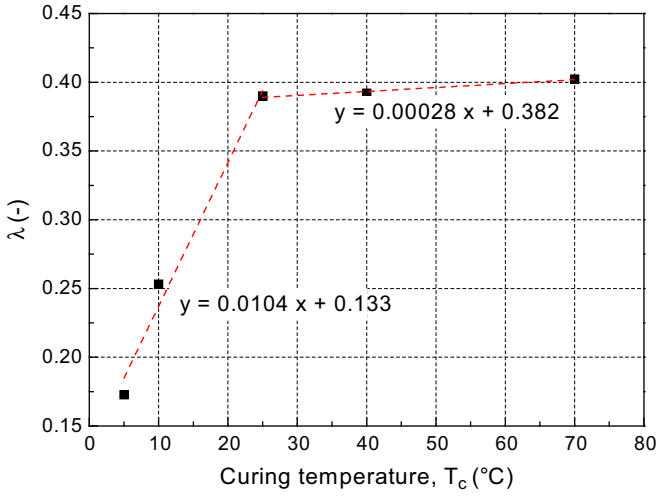

Fig. 11. Modeling parameter λ vs. curing temperature.

6. Consequences for bridge construction

As previously mentioned, bridge construction is performed throughout the whole year and is not interrupted during winter as this would result in unacceptable traffic obstructions. To exploit the benefits of structural adhesive bonding and enable a widespread application of this technique, fast bonding during winter time—at relatively low temperatures—must therefore be possible. Results of this study show, however, that at low temperatures, i.e.

around 5–10 °C, curing develops very slowly. At 5 °C, for example, a curing time of several days is required to attain around 80% cure. Assuming that the mechanical properties develop similarly, this means that the adhesive joint is structurally not yet effective during this period. In most cases, however, such time intervals are not acceptable for just the bonding of structural elements. To accelerate curing therefore, the joint must be designed in such a way that it can be heated and/or that the curing heat cannot easily dissipate. In the case of steel adherends, with relatively high thermal conductivity, the first method seems more suitable while in concrete construction the second method seems more adequate due to the lower thermal conductivity.

Along with curing degree and mechanical properties, the glass transition temperature also develops very slowly. This latter delay however is not as critical as the former because temperatures are low during winter and the T_g will in most cases not be exceeded. Subsequently, in spring, the T_g will develop rapidly with increasing temperature. According to Figs. 9, 3 and 4 days at 25 °C suffice for the maximum value to be attained.

7. Conclusions

The effect of low-temperature curing on the physical characteristics of a commercial cold-curing epoxy adhesive was experimentally and analytically investigated with a view to a potential application in bridge construction during winter. The following conclusions were drawn:

1) Curing did take place at low temperatures of 5–10 °C but the curing process significantly decelerated. Several days of curing were required before high curing degrees of $>80\%$ were reached. The glass transition temperature developed even more slowly due to initiation of vitrification when the low curing temperature was reached.
2) Existing dynamic and isothermal curing models developed for hot-curing adhesives proved applicable to simulate the curing behavior of the cold-curing adhesive even at low temperatures. However, a heating rate-dependent pre-exponential factor and diffusion control had to be taken into account. Accurate modeling results confirmed the autocatalytic behavior exhibited by the cold-curing adhesive.
3) The relationship between the glass transition temperature and the curing degree could also be described by models developed for hot-curing adhesives. However, at low temperatures, the relationship was curing temperature-dependent, something which had to be taken into account in the modeling for accurate simulation.
4) The long curing periods at low temperatures required in winter are in most cases not acceptable in bridge construction. For adhesives to be applied however, joints must be designed in such a way that they are heatable in order to accelerate curing.

In a next step, the development of the mechanical properties of cold-curing adhesives at low temperatures and their dependence on the physical state will be investigated.

Acknowledgments

The authors would like to thank the Federal Authority of Roads and Bridges (FEDRO) for the funding of this project; SIKA AG, Zurich for supplying the adhesive and the Laboratory of Composite and Polymer Technology (LTC – EPFL) for use of the DSC equipment.

References

[1] Dunn DJ. Engineering and structural adhesives. Rapra Rev Rep 2004;15(1):1–28.
[2] Mays GC, Hutchinson AR. Adhesives in Civil Engineering. Cambridge university press; 1992.
[3] 〈http://www.meteoswiss.admin.ch〉 Federal office of meteorology and climatology meteoswiss.
[4] Fiedler E. Die Entwicklung des Stahlbrückenbaues in der DDR bis zum Zeitpunkt derWende ein Rückblick (Teil II). Stahlbau 2001;70(5):317–28.
[5] Buyukozturk O, Bakhoum MM, Beattie SM. Shear behavior of joints in precast concrete segmental bridges. J Struct Eng 1990;116(12):3380–401.
[6] Messler Jr. RW. Joining composite materials and structures: some thought provoking possibility. J Thermoplast Compos Mater 2004;17(1):51–75.
[7] Meier U. Strengthening of structures using carbon fibre/epoxy composite. Constr Build Mater 1995;9(6):341–51.
[8] Motavalli M, Terrasi GP, Meier U. On the behaviour of hybrid aluminium/CFRP box beams at low temperatures. Compos Part A-Appl S 1997;28(2):121–9.
[9] Ellis B. Chemistry and Technology of Epoxy Resins. Blackie academic professional, an imprint of Chapman & Hall; 1993.
[10] Wisanrakkit G, Gillham JK. Glass transition temperature (T_g) as an index of chemical conversion for high-T_g amine/epoxy system: chemical and diffusion-controlled reaction kinetics. J Appl Polym Sci 1990;41(11-12):2885–929.
[11] Boey FYC, Qiang W. Experimental modeling of the cure kinetics of an epoxy–hexahydro-4-methylphthalic anhydride (mhhpa) system. Polym J 2000;41(6):2081–94.
[12] Lee JY, Choi HK, Shim MJ, Kim SW. Kinetic studies of an epoxy cure reaction by isothermal DSC analysis. Thermochim Acta 2000;343(1–2):111–7.
[13] Sun L, Pang S, Sterling. A, Negulescu I, Stubblefield M. Thermal analysis of curing process of Epoxy Prepreg. J Appl Polym Sci 2002;83(5):1074–83.
[14] Chern CS, Phoehlein GW. A kinetic model for curing reactions of epoxides with amines. Polym Eng Sci 1987;27(11):788–95.
[15] Yousefi A, Lafleur PG, Gauvin R. Kinetic studies of thermoset cure reactions: a review. Polym Composite 1997;18(2):157–68.
[16] Atarsia A, Boukhili R. Relationship between isothermal and dynamic cure of thermosets via the isoconversion representation. Polym Eng Sci 2000;40(3):607–20.
[17] Sun L, Pang S, Sterling. A, Negulescu I, Stubblefield M. Dynamic analysis of curing process of Epoxy Prepeg. J Appl Polym Sci 2002;86(8):1911–23.
[18] Kessler MR, White SR. Cure kinetics of the ring opening metathesis polymerization of Dicyclopentadiene. J Polym Sci 2002;40(14):2373–83.
[19] Kissinger HE. Reaction kinetics in differential thermal analysis. Anal Chem 1957;29(11):1702–6.
[20] Ozawa T. A new method of analyzing thermogravimetric data. Bull Chem Soc Jpn 1965;38(11):1881–6.
[21] Ryan ME, Dutta A. Kinetics of epoxy cure: a rapid technique for kinetic parameter estimation. Polym 1979;20(2):203–6.
[22] Pascault JP, Williams RJJ. Relationships between glass transition temperature and conversion—analyses of limiting cases. Polym Bull 1990;24(1):115–21.
[23] Hale A, Macosko CW, Bair HE. Glass transition temperatures as a function of conversion in thermosetting polymers. Macromolecules 1991;24(9):2610–21.
[24] Venditti RA, Gillham JK. A relationship between the glass transition temperature and fractional conversion in thermosetting systems. J Appl Polym Sci 1997;64(1):3–14.
[25] Boey FYC, Qiang W. Glass-transition temperature/conversion relationship for an epoxy–hexahydro-4-methylphthalic anhydride system. J Appl Polym Sci 2000;78(3):511–6.
[26] Dibenedetto AT. Prediction of the glass transition temperature of polymers: a model based on the principal of corresponding states. J. Polym Sci Pt:B Polym Phys 1987;25(9):1949–69.
[27] Couchman PR, Karasz FE. A classical thermodynamic discussion of the effect of composition on glass-transition temperatures. Macromolecules 1978;11(1):117–9.